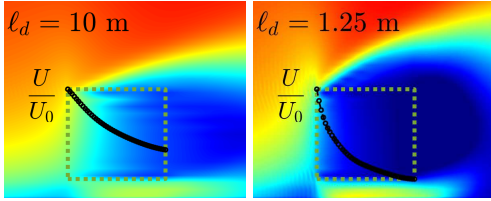


Graphical Abstract

The drag length is key to quantifying tree canopy drag

Dipanjan Majumdar, Giulio Vita, Rubina Ramponi, Nina Glover, Maarten van Reeuwijk



Highlights

The drag length is key to quantifying tree canopy drag

Dipanjana Majumdar, Giulio Vita, Rubina Ramponi, Nina Glover, Maarten van Reeuwijk

- The drag properties of trees are determined by a single drag length $\ell_d = (aC_d^V)^{-1}$ where a is the leaf-area density and C_d^V is the volumetric drag coefficient.
- Field and wind-tunnel measurements with real vegetation find the median drag length to be 21 m for trees and 0.7 m for low vegetation. Whereas median of ℓ_d values used by numerical models and wind-tunnel tree models (assuming geometric scaling 1 : 100) is about 5 m, suggesting possible overestimation of tree drag by these models.
- In order to maintain the same dynamic conditions as at full scale, geometric scaling must be applied to the drag length of model trees in wind tunnels.
- The aerodynamic porosity, often measured in wind-tunnel experiments provides direct access to the drag length ℓ_d and thus to aC_d^V . It is not crucial to have measurement of the actual drag force to determine ℓ_d .

The drag length is key to quantifying tree canopy drag

Dipanjan Majumdar^{a,*}, Giulio Vita^b, Rubina Ramponi^c, Nina Glover^d, Maarten van Reeuwijk^a

^aDepartment of Civil and Environmental Engineering, Imperial College London, South Kensington Campus, London, SW7 2AZ, United Kingdom

^bRTR Advanced Simulations UK, Ramboll UK Ltd., Cornerblock Two, 2 Cornwall St, Birmingham, B3 2DX, United Kingdom

^cSpecialist Technology, Analytics and Research, Arup, 50 Ringsend Road, Dublin, D04 T6X0, Ireland

^dWSP, 3 Wellington Place, Leeds, LS1 4AP, United Kingdom

Abstract

The effects of trees on urban flows are often determined using computational fluid dynamics approaches which typically use a quadratic drag formulation based on the leaf-area density a and a volumetric drag coefficient C_d^V to model vegetation. In this paper, we develop an analytical model for the flow within a vegetation canopy and identify that the drag length $\ell_d = (aC_d^V)^{-1}$ is the key metric to describe the local tree drag characteristics. A detailed study of the literature suggests that the median ℓ_d observed in field experiments is 21 m for trees and 0.7 m for low vegetation (crops). A total of 168 large-eddy simulations are conducted to obtain a closed form of the analytical model. The model allows determining a and C_d^V from wind-tunnel experiments that typically present the drag characteristics in terms of the classical drag coefficient C_d and the aerodynamic porosity α_L . We show that geometric scaling of ℓ_d is the appropriate scaling of trees in wind tunnels. Evaluation of ℓ_d for numerical simulations and wind-tunnel experiments (assuming geometric scaling 1 : 100) in literature shows that the median ℓ_d in both these cases is about 5 m, suggesting possible overestimation of vegetative drag.

Keywords:

trees in urban environment, modelling of tree canopy, drag length, drag coefficient, aerodynamic porosity, wind-break

1. Introduction

Trees are one of the central features of an urban environment. Trees make up at least 10% of the total surface area in most cities and are often referred to as the urban forest (Oke, 1989). Trees make several contributions to the urban ecosystem, in particular flood water mitigation, reduction of heat stress through shading and evapotranspiration, improvement of air quality, and noise reduction (Oke et al., 2017; Bozovic et al., 2017). Trees also play an important role in attenuating pedestrian-level winds (Chen et al., 2021). Indeed, trees are regularly used as wind-breaks (Smith et al., 2021; Weninger et al., 2021).

Wind engineering practitioners have increasingly adopted a computational fluid dynamics (CFD) model approach to model the pedestrian level wind environment and provide feedback on

the thermal comfort and safety conditions for the public. Given their prevalence, it is critical to include vegetation in these simulations (Salim et al., 2015), which presents two distinct challenges. The first is to select an appropriate tree model given their complex interactions with the wind field, temperature, humidity, long- and shortwave radiation, and air quality (e.g. Manickathan et al., 2018; Grylls and van Reeuwijk, 2021). The required complexity of the tree model will depend on the modelling needs of a project – a wind study will require a less complex tree model than an urban microclimate study. The second challenge is – once a suitable tree model has been selected – what the appropriate parameter values are, as these will differ substantially depending on the characteristics of the tree (e.g. species, age, season, etc.).

The drag exerted by trees is typically modelled, within CFD,

*d.majumdar@imperial.ac.uk

Nomenclature

α	Aerodynamic porosity, $\alpha = U/U_0$	c	Velocity shape coefficient, $c = \langle \bar{u}^2 \rangle_{yz} / \langle \bar{u} \rangle_{yz}^2 = \langle \bar{u}^2 \rangle_{yz} / U^2$
α_L	Aerodynamic porosity of the entire tree canopy based on windward and leeward planes, $\alpha_L = \alpha _{x=L} = U_L/U_0$	C_d	Bulk drag coefficient based on projected frontal area, $C_d = 2F_d / (\rho A_F U_\infty^2)$
β	A lengthscale coefficient assumed to be constant along the length of a tree canopy	C_d^V	Volumetric drag coefficient
Δp	Kinematic pressure difference between the windward and leeward sides of the canopy, $\Delta p = p_{ww} - p_{lw}$	Dr	Vegetation drag number, $Dr = H_b / \ell_d$
ℓ_d	Tree drag length, $\ell_d = (aC_d^V)^{-1}$	F_d	Bulk drag force
$\hat{\beta}$	Prediction for β based on regression model	H	Tree canopy crown height from ground, $H = h_0 + h$
$\hat{\ell}_d$	Prediction for ℓ_d by making use of the regression model of β	h	Height of a tree canopy along z -direction
κ	Factor relating bulk drag coefficient and aerodynamic porosity, $\kappa = \frac{C_d}{1 - \alpha_L^2} = c(1 + \beta)(U_0/U_\infty)^2$	h_0	Tree canopy base height from ground
λ	Pressure loss coefficient, $\lambda = 2\Delta p / (U^2 L)$	H_b	Average building height
$\langle \bar{p} \rangle_{yz}$	Average horizontal pressure over the tree frontal area, $\langle \bar{p} \rangle_{yz} = A_F^{-1} \iint_{A_F} \bar{p}(x, y, z) dy dz$	L	Length of a tree canopy along x -direction
ν	Kinematic viscosity of wind	p_{lw}, p_{ww}	Kinematic pressure at leeward and windward sides of the canopy, respectively
\bar{p}	Kinematic pressure, averaged over time	Re	Reynolds number based on the building height, $Re = \frac{U_\infty H_b}{\nu}$
\bar{u}	Streamwise component of wind velocity averaged over time	s	Geometric scaling factor
ρ	Wind density	S_u	Streamwise component of \mathbf{S}_u
\mathbf{u}	Wind velocity vector	$U, \langle \bar{u} \rangle_{yz}$	Streamwise wind velocity averaged over the tree frontal area, $U = \langle \bar{u} \rangle_{yz} = A_F^{-1} \iint_{A_F} \bar{u}(x, y, z) dy dz$
\mathbf{S}_u	Volumetric source/sink term to model trees in CFD simulations, $\mathbf{S}_u = -aC_d^V \mathbf{u} \mathbf{u}$	U_0, U_L	U at windward and leeward planes of a tree canopy, respectively, $U_0 = U _{x=0}$ and $U_L = U _{x=L}$
a	Leaf-area density	U_∞	Free stream wind speed, <i>i.e.</i> , U at a far upstream location
A_F	Projected windward frontal area of a tree canopy	V	Volume of a tree canopy
		W	Width of a tree canopy along y -direction
		x, y, z	Coordinate axes

as a volumetric sink term (\mathbf{S}_u) of momentum with a quadratic dependence on velocity (Shaw and Schumann, 1992; Raupach

et al., 1996; Finnigan, 2000; Nebenführ and Davidson, 2015),

$$\mathbf{S}_u = -aC_d^V |\mathbf{u}| \mathbf{u}, \quad (1)$$

where \mathbf{u} denotes the wind velocity vector (typically the Reynolds-average), a is the leaf-area density (Oke et al., 2017), and C_d^V is the volumetric drag coefficient. Models that are based on the Reynolds-averaged Navier-Stokes equations typically also add terms in the turbulence kinetic energy and dissipation equations (Sanz, 2003; Mochida et al., 2008; Salim et al., 2015; Buccolieri et al., 2018), but importantly these also include a and C_d^V .

Two distinct tree drag regimes can be identified: the extended canopy regime and the wind-break regime. The first is the drag exerted onto the atmosphere by extended forests, where the tree drag is in equilibrium with the vertical divergence of the vertical transport of horizontal momentum by turbulence (Belcher et al., 2008). As a is formally defined as the one-sided leaf area per unit volume of air, this allows for a straightforward calculation of C_d^V . The typical values for both a and C_d^V from literature are listed in Table A.2. The second drag regime comprises wind-breaks which are much shorter (Lyu et al., 2020), *e.g.* a tree line or a small park, where the momentum from incoming wind is reduced by the tree drag. In this case, one often relies on wind-tunnel studies that are able to determine the drag force at high accuracy; after which it is straightforward to calculate a drag coefficient as (Mayhead, 1973; Guan et al., 2003; Cullen, 2005)

$$C_d = \frac{2F_d}{\rho A_F U_\infty^2}, \quad (2)$$

where F_d is the drag force, A_F is the projected frontal area of the tree canopy facing the incoming wind, U_∞ indicates the average wind speed at far upstream, and ρ indicates air density. There are two issues with representing trees using C_d . The first is that the value of C_d is not constant (Table A.3) but has a strong dependence on the aerodynamic porosity (Salim et al., 2015)

$$\alpha(x) = \frac{\iint_{A_F} \bar{u}(x, y, z) dy dz}{\iint_{A_F} \bar{u}(0, y, z) dy dz}. \quad (3)$$

Here it is assumed that the wind velocity is aligned with the x -direction, and the wind-break starts at $x = 0$. Note that α is a function of x which implies that there is no universal value of C_d for trees as is often observed for high Reynolds number bluff body flows. Often wind-tunnel studies report $\alpha_L (= \alpha|_{x=L})$

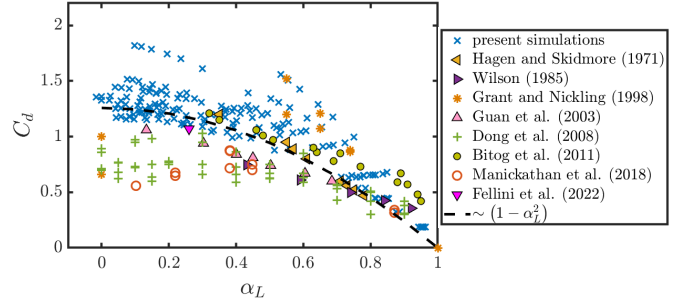


Figure 1: Literature data reflecting overall $C_d \sim (1 - \alpha_L^2)$ behaviour corroborates the proposed model.

which is the ratio of the volume flux on the windward and leeward side of the wind-break (Guan et al., 2003). Figure 1 shows the variation of C_d with respect to α_L reported in literature, along with values obtained from the simulations carried out in this study. There are empirical models that link C_d and α_L (Grant and Nickling, 1998; De-xin et al., 2000; Guan et al., 2003) but these models lack a theoretical basis. The second issue of representing tree drag with Eq. (2) is that it is not clear how the bluff body drag coefficient C_d is related to the volumetric drag coefficient C_d^V . Alternatively, Gromke et al. (2016); Gromke (2018) used a pressure loss coefficient (defined as the static pressure loss per canopy length normalized by the dynamic pressure) to describe the drag induced by the porous foam tree models used in their wind-tunnel experiments. Again, it is not clear how this pressure loss coefficient relates to a and C_d^V .

The accepted value of C_d^V and a in a forest canopy can vary depending on several factors such as tree species, size, age, canopy density, seasonal foliage shedding, and wind conditions. Table A.2 summarises the widely reported values of a and C_d^V ; field and wind-tunnel experiments of real trees indicate that the drag coefficient largely varies within $0.1 \leq C_d^V \leq 3.0$ and the leaf-area density approximately ranges between $0.1 < a < 1.6 \text{ m}^{-1}$ for trees and $1.0 < a < 12.6 \text{ m}^{-1}$ for low vegetation (*e.g.* crops). Although a and C_d^V both varies along the height of the tree foliage, constant values are commonly taken in CFD simulations (Buccolieri et al., 2018; Fu et al., 2024). Instead of species specific values, majority of literature consid-

ers $C_d^V = 0.2$ to reflect an average value for urban vegetation in CFD modelling, and varied the leaf-area density to incorporate seasonal effects; see Table A.2.

As per the tree model in Eq. (1), CFD simulations with a tree canopy require a and C_d^V as the main input parameters to model the tree. However, wind-tunnel experiments with model trees typically measure the quantities C_d and α_L . A direct correlation between a , C_d^V and C_d , α_L is yet to be achieved. Since C_d is defined based on a two-dimension projected area, is fundamentally different from the volumetric coefficient C_d^V . Thus it is not clear what values for a and C_d^V to use as inputs to replicate the same aerodynamic characteristics of an experimental model tree in a corresponding CFD simulation accurately. The present study aims to establish a connection between the two set of parameters in an appropriate manner such that both the CFD and wind-tunnel model trees yield comparable aerodynamic traits. The work will provide an insight into the drag caused by trees on the air flow, and will propose the appropriate parameter values for use in CFD, and how to infer these from wind-tunnel and field data. In order to do so, we construct a simple analytical model for the wind flow inside trees in the wind-break regime (Section 2) and conduct a parametric study using large-eddy simulations (LES) for wind-breaks having various geometric configurations (Section 3). Results are shown in Section 4 and we employ a nonlinear regression to fit a lengthscale parameter in the analytical model. The implications of our findings are discussed in Section 5 and conclusions are made in Section 6.

2. Analytical model for flow inside the tree canopy

Consider a homogeneous vegetation canopy of length L , width W and height h , with the canopy base at height h_0 (Fig. 2). The canopy starts at $x = 0$ where x is in the direction of the wind. The inflow profile is turbulent. The aim is to create an analytical model for the flow inside the canopy.

The starting point of the derivation is a simplified Reynolds-averaged horizontal momentum equation that only considers horizontal advection, the drag exerted by the tree on the fluid,

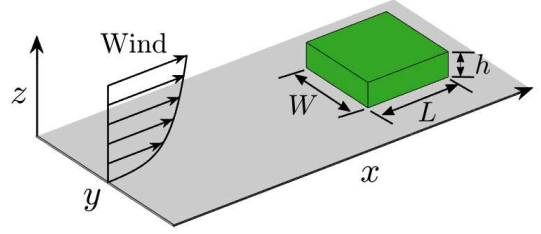


Figure 2: Schematic of a tree canopy.

and the pressure gradient:

$$\bar{u} \frac{\partial \bar{u}}{\partial x} + \frac{\partial \bar{p}}{\partial x} = -a C_d^V \bar{u}^2. \quad (4)$$

Here, u is the wind velocity in x -direction, and p is the kinematic pressure; the overbar sign ($\bar{\cdot}$) indicates the temporal mean. Averaging Eq. (4) over the canopy height and width, and introducing a tree drag length $\ell_d = (a C_d^V)^{-1}$, one obtains

$$\frac{d\langle \bar{u}^2 \rangle_{yz}}{dx} + 2 \frac{d\langle \bar{p} \rangle_{yz}}{dx} = -\frac{2}{\ell_d} \langle \bar{u}^2 \rangle_{yz}, \quad (5)$$

where $\langle * \rangle_{yz} = (Wh)^{-1} \int_{h_0}^{h_0+h} \int_{-W/2}^{W/2} (*) dy dz$. Note that ℓ_d fully characterises the drag properties of the vegetation; this length-scale was found to be the central parameter for the adjustment length in inhomogeneous vegetation canopies (Finnigan and Brunet, 1995; Finnigan, 2000; Banerjee et al., 2013).

Typical ℓ_d values of vegetation canopies as reported by various field- studies, wind-tunnel studies, and simulations in literature are summarised in Table A.2 and are displayed in Fig. 3 as box-plots. Here, we have distinguished between tree canopies and low-vegetation canopies (*i.e.* crops). The data shows that the median value of ℓ_d for trees is 21 m, with an interquartile range of $10 < \ell_d < 34$ m. Low vegetation has a median value of $\ell_d = 0.7$ m with an interquartile range $0.4 < \ell_d < 1.2$ m. Also shown in the figure are the values used in numerical models which show a median value of 4.6 m with an interquartile range of $2.6 < \ell_d < 8.8$ m. We note that this is substantially smaller than the field studies suggest, which in turn might overestimate the effect of trees on wind mitigation. However, note that it is unclear how much the trunks contribute to the drag in the field studies, since trunks are likely to be less important for extended canopies (which are what most of the field

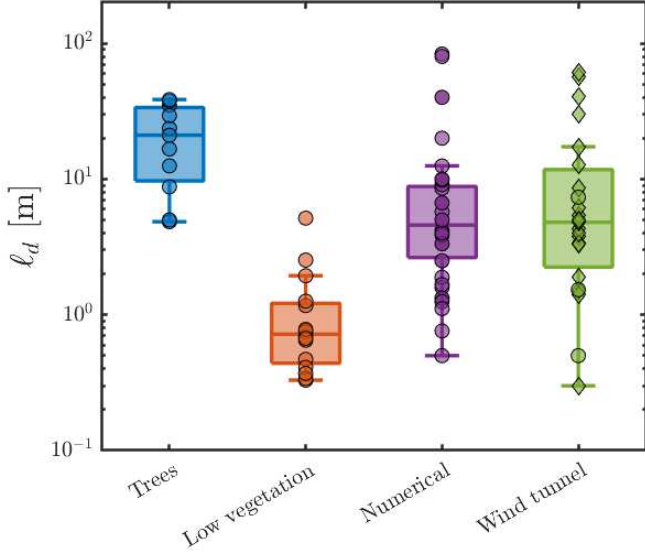


Figure 3: Box-plot of drag length variation for trees, low vegetation, numerical-model trees, and wind-tunnel model trees. Markers indicate the individual data point from Tables A.2 and A.3. The circles indicates full-scale values based on literature and the diamonds represent drag lengths of the wind-tunnel model trees in Table A.3 that have been converted to full-scale values assuming a scaling factor $s = 100$.

studies report on) than for wind-breaks. The figure also shows estimates for wind-tunnel model trees (green colour); the calculation method and results will be discussed in Sections 5.1 and 5.2.

To obtain a solution for Eq. (5), we define the average velocity $U = \langle \bar{u} \rangle_{yz}$, average pressure $P = \langle \bar{p} \rangle_{yz}$ and a shape coefficient $c = \langle \bar{u}^2 \rangle_{yz} / U^2$ which is assumed to be independent of x . With these definitions, Eq. (5) is given by

$$\frac{dU^2}{dx} + \frac{2}{c} \frac{dP}{dx} = -\frac{2}{\ell_d} U^2. \quad (6)$$

We assume that the pressure gradient has the same form as the inertial term inside the tree canopy, *i.e.*,

$$\frac{2}{c} \frac{dP}{dx} = \beta \frac{dU^2}{dx}. \quad (7)$$

This implies that the pressure inside the canopy is assumed to evolve as $P = P_0 + \frac{1}{2} \beta c (U^2 - U_0^2)$, where $P_0 = P|_{x=0}$, $U_0 = U|_{x=0}$, and β is a coefficient assumed to be independent of x . The results will show that this assumption works reasonably well. Although other parameterisations are conceivable, this one stands out for its simplicity. It should be recognised that

the coefficient β represents, apart from the effect of pressure, all three-dimensional effects not included in Eq. (4). With this assumption, Eq. (6) becomes

$$(1 + \beta) \frac{dU^2}{dx} = -\frac{2}{\ell_d} U^2. \quad (8)$$

Together with the boundary condition $U(x = 0) = U_0$, Eq. (8) has the solution

$$U = U_0 \exp\left(-\frac{x}{(1 + \beta)\ell_d}\right), \quad (9)$$

which implies that the aerodynamic porosity α given in Eq. (3) evolves as

$$\alpha = \frac{U}{U_0} = \exp\left(-\frac{x}{(1 + \beta)\ell_d}\right). \quad (10)$$

Small values of $x/\ell_d \ll 1$ are representative of the wind-break regime, and large values of $x/\ell_d \gg 1$ of the continuous canopy regime (where the model Eq. (4) is not valid). Assuming that the wind-break regime is present until U drops to 5% of U_0 , the associated canopy length is $3(1 + \beta)\ell_d$.

The canopy drag force is given by

$$\begin{aligned} F_D &= \rho \int_V S_u dV = \frac{\rho W h c}{\ell_d} \int_0^L U^2 dx \\ &= \frac{1}{2} \rho W h c U_0^2 (1 + \beta) \left\{ 1 - \exp\left(-\frac{2L}{(1 + \beta)\ell_d}\right) \right\}. \end{aligned} \quad (11)$$

Therefore, the drag coefficient defined in Eq. (2) is given by

$$C_d = c(1 + \beta) \left(\frac{U_0}{U_\infty}\right)^2 \left\{ 1 - \exp\left(-\frac{2L}{(1 + \beta)\ell_d}\right) \right\}. \quad (12)$$

Note that C_d attains 95% of its wind-break value in $1.5(1 + \beta)\ell_d$ rather than $3(1 + \beta)\ell_d$, due to its dependence on U^2 . Finally using Eq. (10), C_d can be directly related to the aerodynamic porosity as

$$C_d = \kappa (1 - \alpha_L^2), \quad (13)$$

where $\kappa = c(1 + \beta) (U_0/U_\infty)^2$, and $\alpha_L = \alpha|_{x=L}$. This relation explains why the literature (Hagen and Skidmore, 1971; Wilson, 1985; Grant and Nickling, 1998; Dong et al., 2008) finds such a strong relationship between C_d and α ; see Fig. 1 which summarises the spread in C_d of wind-breaks and trees in relation to α as reported in literature and obtained in the simulations carried out in this work. A notable spread in C_d for a given porosity is due to different tree canopy types, and also because the

method of calculating the aerodynamic porosity varies across the listed studies. According to Eq. (13), C_d starts at 0 when $\alpha_L = 1$, and then increases as $\sim (1 - \alpha_L^2)$ with decreasing α_L . Eventually, C_d reaches a value of κ at $\alpha_L = 0$. These outcomes corroborate well the physical flow behaviour inside a tree canopy as delineated in the literature. Dong et al. (2007) reported a critical value of α_L to be 0.3. Above this critical α_L , there exists a dominant bleed flow through the tree causing the drag force to decrease quickly with increasing α_L . Below critical α_L , there exists only little bleed flow through the tree and most portion of the incoming wind flows around, resulting in a recirculation zone downstream (Manickathan et al., 2018).

In the simplified canopy model proposed here, it is assumed that the cross-section area of the tree canopy remains constant both along its height and length. Moreover, the leaf-area density a is assumed to be constant along the height, and the effect of foliage reconfiguration (Rudnicki et al., 2004; Vollsinger et al., 2005; Manickathan et al., 2018) has been disregarded. These may not be always true for real trees in nature. However, the importance of the proposed theoretical model is that it provides an explicit understanding of the bulk (average) flow behaviour inside the tree canopy. Certainly, the theory can be extended in future taking the spatial variation of the tree properties into consideration. Despite these obvious limitations, the present model provides interesting insights into the determination of the volumetric drag coefficient C_d^V :

- i. Aerodynamic porosity is a proxy for ℓ_d , since $\alpha_L = \alpha|_{x=L} = \exp(-L/(1 + \beta)\ell_d)$. Thus the aerodynamic porosity provides direct access to the drag length ℓ_d . Note that it is unnecessary to determine the actual drag force, although that will of course provide another independent estimate of ℓ_d .
- ii. As far as total drag is concerned, the leaf-area density and the volumetric drag coefficient are exchangeable and combine into a single drag length $\ell_d = (aC_d^V)^{-1}$. The corollary is that a must be determined independently; once this is done, the appropriate value for C_d^V can be obtained using ℓ_d .
- iii. A limitation of the current model is that α is a meaningful quantity only in the wind-break regime as it decays to zero for extended canopies. Measurements of longer canopies do not necessarily provide better information if the canopy length is longer than the wind-break regime $3(1 + \beta)\ell_d$.

Equations (10) and (13) model the overall aerodynamic traits of the vegetation canopy. The former indicates how the bulk flow evolves inside the canopy whereas the latter establishes a direct correlation between α and C_d . However, the coefficient β in Eq. (10) is unclosed and there is insufficient information available in literature to determine it. A combination of both recirculation and bleed flow affects the value of β , and it is likely to depend on L , W , H , ℓ_d , U_∞ , U_0 etc. Additionally, the dominant three-dimensional nature of the flow at low ℓ_d (high aC_d^V) can significantly influence β , as the momentum balance in such situations occurs in the vertical direction instead of the horizontal momentum balance considered in Eq. (4). In order to provide a suitable parameterisation of β , LES is used to carry out a wide parametric study.

3. Simulation details

The simulations are performed using uDALES (Suter et al., 2022; Owens et al., 2024) which is a multi-physics micro-climate modelling framework for the urban environment. It performs LES of the incompressible Navier-Stokes equations within the Boussinesq approximation. The effects of urban surfaces are taken into account in terms of a novel conservative immersed boundary method (Owens et al., 2024). uDALES uses wall functions to model surface fluxes (*e.g.* shear stress) which are then converted to appropriate source/sink terms to apply in the momentum equations. Grylls and van Reeuwijk (2021) included trees in the uDALES framework, modelling the drag, shading, evaporation and deposition. The primary focus in the current work is the drag behaviour under neutral atmospheric conditions. Trees are modeled in uDALES as rectangular blocks, and the source/sink term defined in Eq. (1) is applied to the

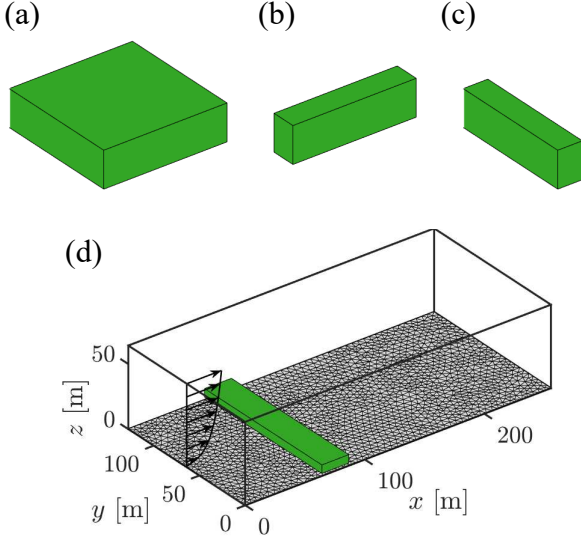


Figure 4: Schematic tree canopy blocks: a) square (S), b) long (L), c) wide (W), and d) infinitely wide (I) tree canopy along with the computational domain.

grid points that fall within the volumetric tree blocks. The turbulence is resolved up to the grid scale and the subgrid-scale turbulence is modelled using the Vreman eddy viscosity (Vreman, 2004). More details on the uDALES framework and the tree modelling can be found in the works of Grylls and van Reeuwijk (2021); Owens et al. (2024).

The default tree geometry is chosen to be a cuboid of size $L \times W \times h = 4.5 \times 4.5 \times 6.5 \text{ m}^3$, taking inspiration from the wind-tunnel experiments of Fellini et al. (2022), resembling the canopy of a single tree. The base of the tree is at $h_0 = 2.0 \text{ m}$ height from the ground, hence the crown of the tree is at a height of $H = h_0 + h = 8.5 \text{ m}$ from the ground. Starting from this default tree geometry, a large parametric study is set up, with canopies categorised as:

- i. square (S): five such cases with $L = W = 4.5 \text{ m}$, 9.0 m , 13.5 m , 18.0 m and 22.5 m ;
- ii. long (L): four such cases with $L = 9.0 \text{ m}$, 13.5 m , 18.0 m and 22.5 m , keeping $W = 4.5 \text{ m}$ fixed;
- iii. wide (W): four such cases with $W = 9.0 \text{ m}$, 13.5 m , 18.0 m and 22.5 m , keeping $L = 4.5 \text{ m}$ fixed;
- iv. infinitely wide tree canopy (I): here the canopy width spanned the entire computational domain width emulating an infinitely wide tree canopy, two such cases with

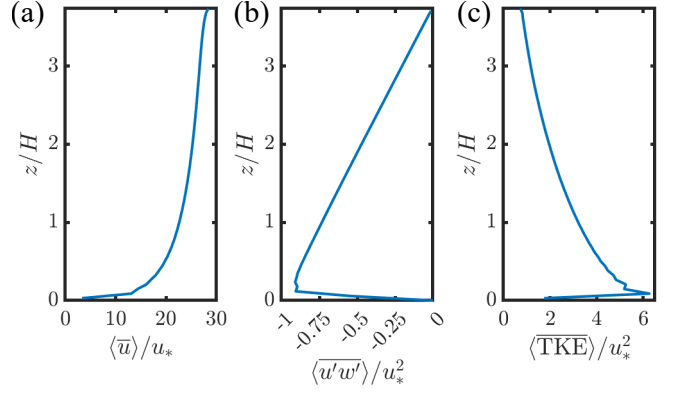


Figure 5: Temporal and spatially averaged profile of the flow-field supplied at the inlet of the simulations with tree canopy; (a) stream-wise velocity, (b) Reynolds stress term, and (c) turbulent kinetic energy. u_* : shear/friction velocity.

$L = 4.5 \text{ m}$ and 22.5 m are considered.

Unless specifically mentioned, the height of the tree canopy is kept constant as $h = 6.5 \text{ m}$. Additionally, a few selected cases are also run with different canopy heights, $h = 13.5 \text{ m}$ and 18.0 m . For each of the above canopy dimensions, aC_d^V is varied such that $aC_d^V \in [0.02, 0.1, 0.2, 0.3, 0.4, 0.6, 0.8, 1.0] \text{ m}^{-1}$, i.e., $\ell_d \in [50.0, 10.0, 5.0, 3.33, 2.5, 1.67, 1.25, 1.0] \text{ m}$, respectively. These values of aC_d^V are selected in a way that they cover the spread of C_d^V and a reported in literature for various types of tree canopies as listed in Table A.2. All simulation cases are systematically summarised in Table 1 for clarity.

The dimension of the computational domain is $256 \times 128 \times 32 \text{ m}^3$, consisting of total $512 \times 256 \times 64$ grid points with approximately 0.5 m uniform grid spacing in all directions. The tree blocks are placed at 64.0 m distance from the inlet, and symmetrically along the y -direction. Schematic diagrams of the computational domain with different types of tree canopies are shown in Fig. 4. The computational domain size is such that the blockage ratio ($= (\text{tree frontal area} / \text{domain frontal area}) \times 100\%$) remains below 5% for the ‘S’, ‘L’ and ‘W’ cases. The ‘I’ cases and the taller canopy cases are run with a larger domain of $256 \times 128 \times 64 \text{ m}^3$ ($512 \times 256 \times 128$ grid points) to maintain the acceptable limit of 10% blockage ratio. Obviously, the tree canopies being porous in nature, flow can pass through them, as a result, the actual blockage ratio is less than what one ob-

Table 1: Summary of the total 168 different simulation cases.

Type	Canopy size	Canopy length / Drag length								
	$L \times W \times h$ [m ³]	L/ℓ_d [-]								
S45	4.5 × 4.5 × 6.5	0.09, 0.45, 0.90, 1.35, 1.80, 2.70, 3.60, 4.50								
S90	9.0 × 9.0 × 6.5	0.18, 0.90, 1.80, 2.70, 3.60, 5.40, 7.20, 9.00								
S135	13.5 × 13.5 × 6.5	0.27, 1.35, 2.70, 4.05, 5.40, 8.10, 10.8, 13.5								
S180	18.0 × 18.0 × 6.5	0.36, 1.80, 3.60, 5.40, 7.20, 10.8, 14.4, 18.0								
S225	22.5 × 22.5 × 6.5	0.45, 2.25, 4.50, 6.75, 9.00, 13.5, 18.0, 22.5								
L90	9.0 × 4.5 × 6.5	0.18, 0.90, 1.80, 2.70, 3.60, 5.40, 7.20, 9.00								
L135	13.5 × 4.5 × 6.5	0.27, 1.35, 2.70, 4.05, 5.40, 8.10, 10.8, 13.5								
L180	18.0 × 4.5 × 6.5	0.36, 1.80, 3.60, 5.40, 7.20, 10.8, 14.4, 18.0								
L225	22.5 × 4.5 × 6.5	0.45, 2.25, 4.50, 6.75, 9.00, 13.5, 18.0, 22.5								
W90	4.5 × 9.0 × 6.5	0.09, 0.45, 0.90, 1.35, 1.80, 2.70, 3.60, 4.50								
W135	4.5 × 13.5 × 6.5	0.09, 0.45, 0.90, 1.35, 1.80, 2.70, 3.60, 4.50								
W180	4.5 × 18.0 × 6.5	0.09, 0.45, 0.90, 1.35, 1.80, 2.70, 3.60, 4.50								
W225	4.5 × 22.5 × 6.5	0.09, 0.45, 0.90, 1.35, 1.80, 2.70, 3.60, 4.50								
I45	4.5 × 128 × 6.5	0.09, 0.45, 0.90, 1.35, 1.80, 2.70, 3.60, 4.50								
I225	22.5 × 128 × 6.5	0.45, 2.25, 4.50, 6.75, 9.00, 13.5, 18.0, 22.5								
S225H135	22.5 × 22.5 × 13.5	0.45, 2.25, 4.50, 6.75, 9.00, 13.5, 18.0, 22.5								
S225H180	22.5 × 22.5 × 18.0	0.45, 2.25, 4.50, 6.75, 9.00, 13.5, 18.0, 22.5								
S135H135	13.5 × 13.5 × 13.5	0.27, 1.35, 2.70, 4.05, 5.40, 8.10, 10.8, 13.5								
S135H180	13.5 × 13.5 × 18.0	0.27, 1.35, 2.70, 4.05, 5.40, 8.10, 10.8, 13.5								
L135H135	13.5 × 4.5 × 13.5	0.27, 1.35, 2.70, 4.05, 5.40, 8.10, 10.8, 13.5								
W135H135	4.5 × 13.5 × 13.5	0.09, 0.45, 0.90, 1.35, 1.80, 2.70, 3.60, 4.50								

tains based on the frontal area. Unless specifically mentioned, a prescribed inflow and a convective outflow boundary conditions are used in the x -direction, while the y -direction is periodic, and the top is free-slip. At the bottom, no-slip boundary condition is used with a flat ground surface having roughness length 0.05 m. A precursor (driver) simulation (Suter et al., 2022; Owens et al., 2024) with an empty domain is carried out first to generate a neutral turbulent atmospheric boundary layer which is then provided as inflow to the target simulations with tree canopy. The driver simulation is performed with an assigned constant volume flow rate forcing in the x -direction enforcing a bulk wind speed of 1.0 m/s, and with periodic boundary condition in both x and y -directions. Temporally and spatially averaged stream-

wise velocity, Reynolds stress and turbulent kinetic energy profiles obtained from the driver simulation output are shown in Fig. 5. This output velocity data obtained from the driver simulation is provided as inlet in the target simulations with the tree canopy.

4. Results

For a qualitative visualization of the flow inside a tree canopy, we first present the mean streamwise wind velocity and the turbulent kinetic energy, $\text{TKE} = 0.5 (\overline{u'u'} + \overline{v'v'} + \overline{w'w'})$, contours at the mid-span vertical plane for typical representative cases at $\ell_d = 3.33$ m; see Fig. 6. The overall qualitative characteristics of the flow through the tree canopy remain the same for

all the canopy types. The presence of the tree slows down the incoming flow as it enters into the canopy. Both flow velocity and TKE decay close to zero towards the leeward side of the canopy that has L (22.5 m) sufficiently longer than ℓ_d (3.33 m) satisfying the condition of continuous canopy $L > 3(1 + \beta)\ell_d$; see cases S225, L225 and I225 in Fig. 6. However, for the canopy W225, the flow velocity does not reach zero at the leeward plane, though it exhibits the decaying trend being consistent with the other cases. In W225, the canopy length (4.5 m) is of a similar order of drag length (3.33 m) and is within the wind-break regime $L < 3(1 + \beta)\ell_d$.

To aid quantitative understanding, the variation of aerodynamic porosity along the length of the tree canopy is presented in Fig. 7 for a few typically chosen cases. Note that the evolution of α computed from the simulation output indeed reflects an exponential decay reasonably well and thus supports Eq. (10) and the theoretical model proposed in Section 2.

The coefficient β in Eq. (10) can be estimated by extracting $\alpha(x)$ from the wind velocity data inside the canopy. For each of the 168 simulations, an appropriate value of β has been obtained, that best fits Eq. (10) to the α^2 variation measured from simulation output velocity field. Here, α^2 is considered instead of α , because C_d has direct impact from α^2 (Eq. (13)).

Having obtained β for each simulation, a regression analysis was performed. Applying the Buckingham-Pi theorem to the relation $\beta = f(L, W, H, \ell_d, U_\infty, U_0)$, we expect that $\beta = g(L/\ell_d, W/\ell_d, H/\ell_d, U_\infty/U_0)$. Subsequently, a regression analysis was carried out assuming a power-law relation of the identified dimensionless quantities using the MATLAB function `fminsearch`. Here, only cases for which $\alpha_L > 0.3$ were considered (0.3 being the critical aerodynamic porosity; Dong et al., 2007). The nonlinear fit that minimizes the error norm is given by

$$\hat{\beta} = 0.27 + 0.55 \left(\frac{WH}{\ell_d^2} \right)^{0.33}, \quad (14)$$

where $\hat{\beta}$ indicates the regression fit for β . Note that WH corresponds to the frontal area A_F . The regression relation in Eq. (14) is a function of the projected frontal area and the drag length

only, and not on L/ℓ_d or U_∞/U_0 .

In order to test the accuracy of this approximate model, $\hat{\beta}$ was estimated based on the input L , W and ℓ_d for all the 168 simulation cases, and then the evolution of α was predicted as per Eq. (10). These model predictions are shown in terms of ‘orange-dotted’ lines in Fig. 7. A reasonably good agreement is evident. Additionally, the model predicted α_L^2 are plotted against its value computed from the simulation output wind velocity data in Fig. 8, showing mean absolute error (MAE) and root mean square error (RMSE) of only 0.023 and 0.031, respectively. $\alpha_{L_{\text{model}}}^2$ and $\alpha_{L_{\text{DALES}}}^2$ exhibit reasonably good match, establishing a good confidence on the proposed regression model. Next, we discuss what are implications of the theoretical model proposed in Section 2 and the regression model in Eq. (14), and how these can be put to use in practice.

5. Implications

5.1. Linking wind-tunnel experiments to CFD simulations

The analytical model can be used to estimate ℓ_d of model trees used in wind-tunnel experiments. These experiments typically report C_d and α_L (Table A.3). As pointed out in Section 2, α_L alone is sufficient to estimate the corresponding drag length. Indeed, rearranging Eq. (10) and substituting Eq. (14) leads to

$$\hat{\ell}_d \left[1.27 + 0.55 \left(\frac{WH}{\hat{\ell}_d^2} \right)^{0.33} \right] = -\frac{2L}{\ln(\alpha_L^2)}, \quad (15)$$

which is an implicit equation in $\hat{\ell}_d$ that can be solved using a root finding method. The measurement of bulk drag coefficient is redundant here. The representative values for L , W and H , and α_L can be measured for a model tree in a wind-tunnel experiment and then can be used to obtain $\hat{\ell}_d$ using Eq. (15). This estimated value of ℓ_d can then be used as input to model the tree in a corresponding CFD simulation to replicate the same drag behaviour. We calculated $\hat{\ell}_d$ for a series of wind-tunnel tree models from literature and summarise them in Table A.3. $\hat{\ell}_d$ for different scaled wind-tunnel tree models ranges between 0.003-0.6 m approximately. The present study recommends using ℓ_d estimated from Eq. (15) to model a tree in CFD simulations as

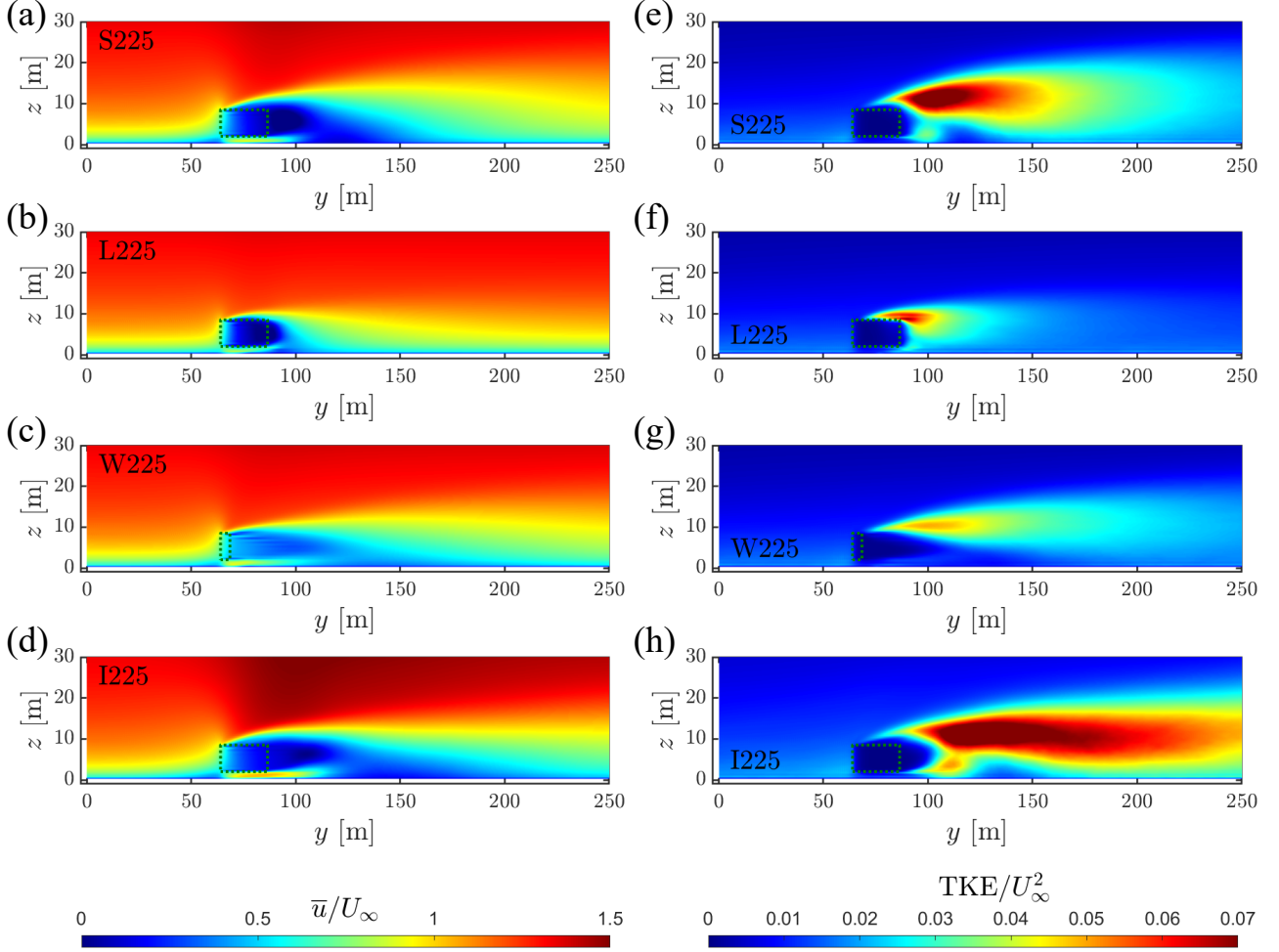


Figure 6: Contour of mean (a-d) streamwise velocity and (e-h) turbulent kinetic energy at the mid-span vertical plane at $\ell_d = 3.33$ m for a representative case from each canopy type.

this equation is obtained based on the wind velocity (a direct flow-field variable) inside the tree canopy, instead of estimating ℓ_d from an average quantity like C_d . Note that for lower aerodynamic porosity ($\alpha_L < 0.3$) caused either by long canopy length or due to higher drag length, $\ln(\alpha_L^2)$ becomes extremely sensitive to the value of α_L , which may lead to erroneous prediction of ℓ_d using Eq. (15), and the model should be used with caution.

5.2. Appropriate scaling for model trees in wind tunnel

Having inferred ℓ_d from the wind-tunnel experiments, it becomes possible to argue what the appropriate scaling should be for trees in wind tunnels. To this extent, we non-dimensionalise the Navier-Stokes equations using a characteristic building height

H_b and velocity U_∞ , which results in

$$\frac{D\mathbf{u}}{Dt} = -\nabla p + \frac{1}{Re} \nabla^2 \mathbf{u} - Dr |\mathbf{u}| \mathbf{u} + \mathbf{f}, \quad (16)$$

where $Re = U_\infty H_b / \nu$ is the Reynolds number (ν is the kinematic viscosity), and Dr is the vegetation drag number defined as

$$Dr = \frac{H_b}{\ell_d}. \quad (17)$$

Wind tunnels often use geometric scaling, *i.e.*, all geometrical dimensions are scaled down by a factor s . Ideally all dimensionless quantities, Re and Dr , in this case would kept identical to achieve full similarity. However, it is typically not possible to achieve the same values of Re in wind tunnels as in reality, but this is not of much concern as Re does not play a crucial role in the urban settings provided it is larger than 10^3 based on

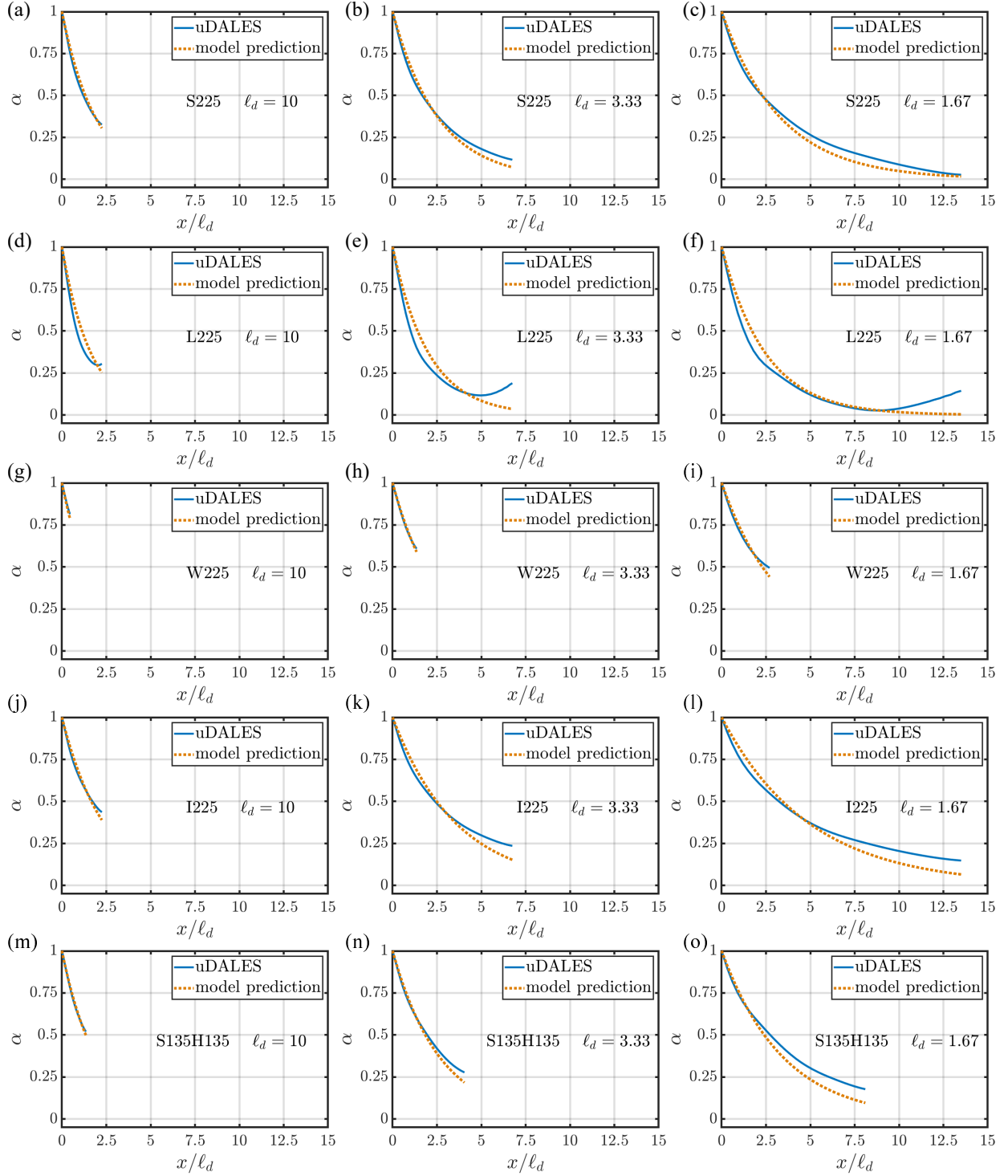


Figure 7: Evolution of aerodynamic porosity inside the tree canopy: actual values obtained from simulation versus model prediction for a set of typically chosen cases. Other cases follow the similar trend as well, and not shown here only for the sake of brevity.

the building height (Shu et al., 2020). In order to achieve similarity for the vegetative drag, Dr should have the same value at both model scale (MS) and full scale (FS): In order to perform the wind-tunnel measurements under the same conditions as in

reality, the drag length should scale by the factor s as well in order to maintain the same value of Dr , *i.e.*,

$$\frac{H_b}{\ell_d} \Big|_{\text{MS}} = \frac{H_b}{\ell_d} \Big|_{\text{FS}} \Leftrightarrow \frac{\ell_{d;\text{MS}}}{\ell_{d;\text{FS}}} = \frac{H_{b;\text{MS}}}{H_{b;\text{FS}}} = \frac{1}{s}, \quad (18)$$

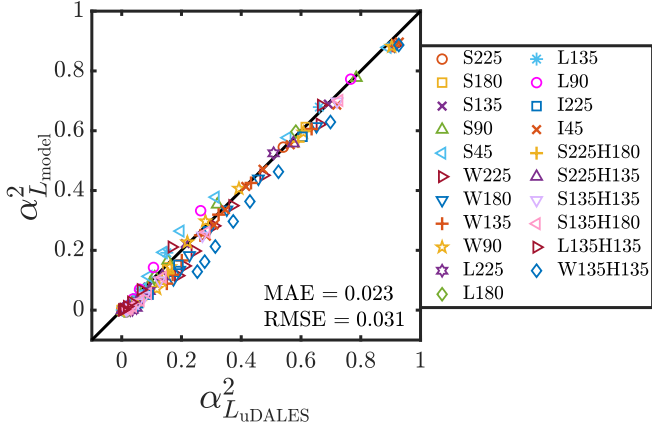


Figure 8: Comparison of model prediction and the values obtained from simulation for the square of aerodynamic porosity. MAE: mean absolute error; RMSE: root mean squared error.

and thus similarity requires that $\ell_{d;MS} = \ell_{d;FS}/s$.

The typical scaling factor s in wind tunnels is 100–400 (Wang et al., 1996; Gromke et al., 2016; Gromke, 2018). From Table A.2 and Fig. 3, the median of full-scale $\ell_{d;FS}$ of trees is 21 m with interquartile range of 10 to 34 m. Based on the arguments above, for a wind tunnel with a scaling factor of 100, $\ell_{d;MS}$ needs to be within the interquartile range of 0.1 – 0.34 m with median of 0.21 m. For a scaling factor of 400, $\ell_{d;MS}$ needs to be within the interquartile range of 0.025 – 0.085 m with median 0.05 m. From the estimated drag lengths of scaled model trees in Table A.3, the median of $\ell_{d;MS}$ is approximately 0.05 m with an interquartile range of 0.03 – 0.15 m. This confirms that trees used in the wind-tunnel experiments have drag length overall falling within the range mentioned above, albeit being on the lower side in comparison to real trees for $s = 100$, suggesting the effects of vegetation on drag may be overestimated by wind-tunnel models.

The argument for wind-tunnel scaling put forward here is consistent with that of Gromke et al. (2016); Gromke (2018), as demonstrated below. They use foam to represent tree canopies and infer its properties by measuring the pressure loss across a foam model of thickness L that spans the entire wind-tunnel cross-section. They determine a pressure loss coefficient λ defined as (Gromke et al., 2016; Gromke, 2018; Buccolieri et al.,

2018)

$$\lambda = \frac{2\Delta p}{U^2 L} \quad (19)$$

where $\Delta p = p_{ww} - p_{lw}$ is the kinematic pressure difference between the windward and leeward sides of the foam. Note that λ has unit m^{-1} .

As the foam covers the entire cross-section, the mean velocity U will remain constant and the momentum balance in Eq. (6) simply becomes

$$\frac{1}{c} \frac{\Delta p}{L} = \frac{1}{\ell_d} U^2. \quad (20)$$

Rearranging and substituting Eq. (19) yields

$$\ell_d = \frac{cU^2 L}{\Delta p} = 2c\lambda^{-1}, \quad (21)$$

which shows that the drag length ℓ_d is simply the inverse of the pressure loss coefficient λ up to a constant.

Covering the entire cross-section with porous material is a smart way to avoid three-dimensional flow effects that normal canopies will create otherwise. It offers a straightforward manner to determine ℓ_d without having to involve the model developed in this paper. However, if one wants to determine ℓ_d of trees including trunks it will be impossible to cover the entire wind tunnel uniformly and the method developed in this paper will be preferable.

5.3. Wind engineering

Wind engineering practitioners have increasingly adopted a numerical (CFD) approach to model the pedestrian level wind environment and provide feedback on comfort and safety conditions for the public. These studies are part of several councils' strategies to improve the liveability of cities, as they become denser and taller due to a rapid increase in urbanisation. A notable case in the UK is the City of London, that recently defined specific Wind Microclimate Guidelines for new developments in their borough (City of London Corporation, 2019).

One of the key aspects of wind microclimate studies is the development and assessment of wind mitigation measures to resolve or dissipate any excessive windiness in and around the

area of interest. Practitioners rely on CFD models, often steady-state, to quantify the effectiveness of these mitigations in comparison with the baseline (unmitigated) situation. The mitigation measures include small elements, however, their geometric and aerodynamic properties are hard to reproduce in urban CFD models and may lead to large uncertainties in the results. This is particularly true for porous elements such as trees and vegetation. Among the many sources of uncertainties in commercial CFD models of trees, some are related to the choice of appropriate aerodynamic parameters, on their use in the numerical model (particularly in the turbulence terms), and on the sensitivity to the grid resolution.

Due to the lack of specific guidelines in the market, the choice of appropriate parameters to describe the aerodynamic properties of vegetation is up to the modeller. Table A.2 illustrates the large variability of a and C_d^V found in literature, which inevitably leads to inconsistencies in simulation results from different providers. This paper introduces a way to combine these variables into the drag length ℓ_d , a physically meaningful lengthscale that describes the spatial extent to which the tree exerts influence on the wind. By consolidating the input values into one parameter, the drag length has the potential to reduce the spread in the results. However, further work is needed to provide an extensive dataset and guidelines for practitioners to enable a wider understanding and use of ℓ_d in different situations.

One pertinent problem is that a formally only provides information about the leaves. For wind engineering applications, the trunks are also of importance, particularly since winter situations with leave-less trees are typically used to quantify the effect of vegetation on wind microclimate. Here, the drag length ℓ_d is highly beneficial, since it directly quantifies the drag, and the parameters C_d^V and a simply need to be set such that the appropriate value of ℓ_d is obtained. For winter-scenarios, this might involve taking a normal value for C_D^V (say 0.2) and then calculating the leaf-area density as $(C_d^V \ell_d)^{-1}$. In CFD simulations of summer scenarios that include tree's evaporative processes, it is paramount the correct value of a is used, and thus

C_d^V can be set as $(a\ell_d)^{-1}$ to capture both drag and evaporation appropriately.

Furthermore, the drag length ℓ_d is likely dependent on the wind speed. Indeed, it is well known that trees undergo foliage reconfiguration at high wind speeds (Bekkers et al., 2022), which creates a strong dependence of C_d^V on wind velocity (Manickathan et al., 2018). For this reason some authors propose to use a streamlining coefficient to be combined with C_d^V , depending on structural properties of the tree crown (Rudnicki et al., 2004; Vollsinger et al., 2005; Manickathan et al., 2018).

A considerable source of uncertainty in commercial tree simulations is the strong dependency of the results on the grid resolution in the topology representing a tree in the CFD model. The concept of drag length ℓ_d is linked to how rapidly the flow is retarded inside the tree canopy. This explicit connection between the tree aerodynamic properties and their effects on the flow can provide useful insights to the minimum grid resolution that is needed to resolve the flow in the area surrounding the tree, which would be some fraction of ℓ_d . This could be very valuable for the industry and guide the definition of specific guidelines for tree modelling in CFD. We thus recommend further work to be carried out that explores the grid requirements due to vegetation with simulation codes used by practitioners.

6. Conclusions

This study developed an analytical model to evaluate drag characteristics of wind-breaks. The model identifies a critical drag parameter, namely the drag length $\ell_d = (aC_d^V)^{-1}$. Here, a is the leaf-area density and C_d^V is a volumetric drag coefficient, not to be confused with the classical (bulk) drag coefficient C_d that is often determined based on projected frontal area in wind-tunnel experiments of vegetation. A detailed study of the literature, summarised in Table A.2, demonstrates that the median value of ℓ_d observed in field experiments is 21 m. The median value of ℓ_d for low vegetation (*e.g.* crops) is 0.7 m. For tree canopy and low vegetation, there is a substantial spread in the data.

The analytical model clearly shows that the bulk drag coefficient C_d is linked to the aerodynamic porosity α as $C_d \sim (1 - \alpha^2)$, providing an explanation for the strong correlation between these parameters observed in wind-tunnel studies. The extensive parametric LES investigation conducted in this work allowed to obtain a closed form of the analytical model, which permits the direct translation between wind-tunnel experiments (that tend to determine C_d and α) and CFD simulations (which require a and C_d^V). This makes it possible to understand what values for a and C_d^V are required to perform simulations of wind-tunnel experiments, and vice versa. The calculation of ℓ_d for a substantial number of wind-tunnel experiments was performed in Table A.3. Median ℓ_d is 0.05 m with an interquartile range 0.03 – 0.15 m for the scaled tree models in wind tunnels.

The identification of the drag length ℓ_d provides clarity on what scaling needs to be used for trees in wind-tunnel experiments. Through the non-dimensionalisation of the Navier-Stokes equations, it is possible to derive a dimensionless vegetation drag number $Dr = \ell_d/H_b$, with H_b a characteristic length of the problem. Geometric scaling would therefore need to be applied to ℓ_d as well in order to achieve the same dynamic conditions as at full scale. A comparison with the work of Gromke et al. (2016); Gromke (2018) showed full consistency with the scaling proposed in that work.

In the context of wind engineering, the introduction of a new vegetation metric would bring about significant benefits to the current status quo. Indeed, reducing the uncertainty in tree modelling is essential if we wish to include trees in wind mitigation schemes with confidence. Future efforts should focus on expanding the dataset of drag length values across various tree species and sizes, as well as accounting for seasonal variations in deciduous trees. By doing so, wind engineers will be better equipped to integrate trees and vegetation into their mitigation designs, enhancing not only wind comfort but also delivering valuable environmental co-benefits.

Author contributions

D.M. and M.v.R. conceptualized the research idea. D.M. contributed to the analytical model development and carried out the literature survey, numerical simulations, data analysis, figure production (Sects. 2, 3, 4, 5.1, Appendix A). G.V., R.R. and N.G. contributed to the discussion in the context of wind engineering (Sect. 5.3). M.v.R. acquired funding, supervised the project as a whole and conceived of the analytical model (Sect. 2) and its implications (Sects. 5.1, 5.2, 5.3). All the authors contributed in preparing and reviewing the manuscript.

Acknowledgements

D.M. acknowledges financial support through the Turbulence at the Exascale project (EP/W026686/1) which is part of the ExCALIBUR HPC programme funded by EPSRC. M.v.R. and D.M. appreciate useful discussions with Prof. Pietro Salizzoni and Dr. Sofia Fellini about the implications of this work for wind-tunnel experiments. This work was inspired by the guide we are developing on CFD of vegetated urban areas as part of the UK Urban Environment Quality (UKUEQ) initiative which is supported by the Wind Engineering Society and CIBSE.

Appendix A. Drag coefficients in literature

The typical values of the volumetric drag coefficient and leaf-area density for various types of vegetation canopies are summarised in Table A.2. The table includes measurements based on field studies and wind-tunnel experiments of different vegetation species, as well as values used in numerical simulations for modelling vegetation canopies in urban areas. The corresponding drag length for each of these cases can be directly computed as $(aC_d^V)^{-1}$; see Table A.2. In Table A.3, we infer the drag length of the model trees used in different wind-tunnel studies. Based on the tree dimension and aerodynamic porosity mentioned in these studies, the corresponding values of $\hat{\ell}_d$ are estimated by solving Eq. (15) numerically using the MATLAB function `solve`. The bulk drag coefficient values are

redundant in this context. The $\hat{\ell}_d$ values can be directly used to replicate these wind-tunnel studies in CFD simulations.

References

- Amiro, B., 1990. Drag coefficients and turbulence spectra within three boreal forest canopies. *Boundary-Layer Meteorology* 52, 227–246.
- Amorim, J., Rodrigues, V., Tavares, R., Valente, J., Borrego, C., 2013. Cfd modelling of the aerodynamic effect of trees on urban air pollution dispersion. *Science of the Total Environment* 461, 541–551.
- Baldocchi, D.D., Meyers, T.P., 1988. A spectral and lag-correlation analysis of turbulence in a deciduous forest canopy. *Boundary-Layer Meteorology* 45, 31–58.
- Banerjee, T., Katul, G., Fontan, S., Poggi, D., Kumar, M., 2013. Mean flow near edges and within cavities situated inside dense canopies. *Boundary-layer meteorology* 149, 19–41.
- Bekkers, C.C., Angelou, N., Dellwik, E., 2022. Drag coefficient and frontal area of a solitary mature tree. *Journal of Wind Engineering and Industrial Aerodynamics* 220, 104854.
- Belcher, S., Finnigan, J., Harman, I., 2008. Flows through forest canopies in complex terrain. *Ecological Applications* 18, 1436–1453.
- Bitog, J., Lee, I.B., Hwang, H.S., Shin, M.H., Hong, S.W., Seo, I.H., Mostafa, E., Pang, Z., 2011. A wind tunnel study on aerodynamic porosity and wind-break drag. *Forest Science and technology* 7, 8–16.
- Bozovic, R., Maksimovic, C., Mijic, A., Smith, K., Suter, I., Van Reeuwijk, M., 2017. Blue green solutions, a systems approach to sustainable, resilient and cost-efficient urban development. Technical Report, Climate-KIC, London: Imperial College, UK .
- Buccolieri, R., Santiago, J.L., Rivas, E., Sanchez, B., 2018. Review on urban tree modelling in cfd simulations: Aerodynamic, deposition and thermal effects. *Urban Forestry & Urban Greening* 31, 212–220.
- Chen, T., Yang, H., Chen, G., Lam, C.K.C., Hang, J., Wang, X., Liu, Y., Ling, H., 2021. Integrated impacts of tree planting and aspect ratios on thermal environment in street canyons by scaled outdoor experiments. *Science of The Total Environment* 764, 142920.
- City of London Corporation, 2019. Wind microclimate guidelines for developments in the city of London. <https://www.cityoflondon.gov.uk/assets/Services-Environment/wind-microclimate-guidelines.pdf>. Accessed: 25-Oct-2024.
- Cullen, S., 2005. Trees and wind: A practical consideration of the drag equation velocity exponent for urban tree risk management. *Arboriculture & Urban Forestry (AUF)* 31, 101–113.
- De-xin, G., Ting-yao, Z., Shi-jie, H., 2000. Wind tunnel experiment of drag of isolated tree models in surface boundary layer. *Journal of Forestry Research* 11, 156–160.
- Dong, Z., Luo, W., Qian, G., Wang, H., 2007. A wind tunnel simulation of the mean velocity fields behind upright porous fences. *Agricultural and Forest Meteorology* 146, 82–93.
- Dong, Z., Mu, Q., Luo, W., Qian, G., Lu, P., Wang, H., 2008. An analysis of drag force and moment for upright porous wind fences. *Journal of Geophysical Research: Atmospheres* 113.
- Duan, G., Bi, Z., Zhao, L., Yang, T., Takemi, T., 2024. Modulating local winds and turbulence around a single building obstacle with the obstruction of tall vegetation. *Physics of Fluids* 36.
- Fellini, S., Marro, M., Del Ponte, A.V., Barulli, M., Soulhac, L., Ridolfi, L., Salizzoni, P., 2022. High resolution wind-tunnel investigation about the effect of street trees on pollutant concentration and street canyon ventilation. *Building and Environment* 226, 109763.
- Finnigan, J., 2000. Turbulence in plant canopies. *Annual review of fluid mechanics* 32, 519–571.
- Finnigan, J.J., Brunet, Y., 1995. Turbulent airflow in forests on flat and hilly terrain. *Wind and trees* , 3–40.
- Fu, R., Padjen, I., Garcia-Sanchez, C., 2024. Should we care about the level of detail in trees when running urban microscale simulations? *Sustainable Cities and Society* 101, 105143.
- Gardiner, B.A., 1994. Wind and wind forces in a plantation spruce forest. *Boundary-Layer Meteorology* 67, 161–186.
- Ghasemian, M., Amini, S., Princevac, M., 2017. The influence of roadside solid and vegetation barriers on near-road air quality. *Atmospheric Environment* 170, 108–117.
- Grant, P., Nickling, W., 1998. Direct field measurement of wind drag on vegetation for application to windbreak design and modelling. *Land Degradation & Development* 9, 57–66.
- Gromke, C., 2018. Wind tunnel model of the forest and its reynolds number sensitivity. *Journal of Wind Engineering and Industrial Aerodynamics* 175, 53–64.
- Gromke, C., Blocken, B., 2015a. Influence of avenue-trees on air quality at the urban neighborhood scale. part i: Quality assurance studies and turbulent schmidt number analysis for rans cfd simulations. *Environmental Pollution* 196, 214–223.
- Gromke, C., Blocken, B., 2015b. Influence of avenue-trees on air quality at the urban neighborhood scale. part ii: Traffic pollutant concentrations at pedestrian level. *Environmental Pollution* 196, 176–184.
- Gromke, C., Blocken, B., Janssen, W., Merema, B., van Hooff, T., Timmermans, H., 2015. Cfd analysis of transpirational cooling by vegetation: Case study for specific meteorological conditions during a heat wave in arnhem, netherlands. *Building and environment* 83, 11–26.
- Gromke, C., Jamarkattel, N., Ruck, B., 2016. Influence of roadside hedgerows on air quality in urban street canyons. *Atmospheric environment* 139, 75–86.
- Grylls, T., van Reeuwijk, M., 2021. Tree model with drag, transpiration, shading and deposition: Identification of cooling regimes and large-eddy simulation. *Agricultural and Forest Meteorology* 298, 108288.
- Grylls, T., van Reeuwijk, M., 2022. How trees affect urban air quality: It depends on the source. *Atmospheric Environment* 290, 119275.
- Guan, D., Zhang, Y., Zhu, T., 2003. A wind-tunnel study of windbreak drag. *Agricultural and forest meteorology* 118, 75–84.

- Hagen, L., Skidmore, E., 1971. Windbreak drag as influenced by porosity. *Transactions of the ASAE* 14, 464–465.
- Jeanjean, A.P., Buccolieri, R., Eddy, J., Monks, P.S., Leigh, R.J., 2017. Air quality affected by trees in real street canyons: The case of Marylebone neighbourhood in central London. *Urban Forestry & Urban Greening* 22, 41–53.
- Katul, G.G., Mahrt, L., Poggi, D., Sanz, C., 2004. One-and two-equation models for canopy turbulence. *Boundary-layer meteorology* 113, 81–109.
- Kenjereš, S., ter Kuile, B., 2013. Modelling and simulations of turbulent flows in urban areas with vegetation. *Journal of Wind Engineering and Industrial Aerodynamics* 123, 43–55.
- Krayenhoff, E., Santiago, J.L., Martilli, A., Christen, A., Oke, T., 2015. Parametrization of drag and turbulence for urban neighbourhoods with trees. *Boundary-Layer Meteorology* 156, 157–189.
- Lee, J.P., Lee, E.J., Lee, S.J., 2014. Shelter effect of a fir tree with different porosities. *Journal of Mechanical Science and Technology* 28, 565–572.
- Li, Z., Miller, D., Lin, J., 1985. A first-order closure scheme to describe counter-gradient momentum transport in plant canopies. *Boundary-layer meteorology* 33, 77–83.
- Liang, L., Xiaofeng, L., Borong, L., Yingxin, Z., 2006. Improved $k-\epsilon$ two-equation turbulence model for canopy flow. *Atmospheric Environment* 40, 762–770.
- Lyu, J., Wang, C.M., Mason, M.S., 2020. Review of models for predicting wind characteristics behind windbreaks. *Journal of Wind Engineering and Industrial Aerodynamics* 199, 104117.
- Manickathan, L., Defraeye, T., Allegrini, J., Derome, D., Carmeliet, J., 2018. Comparative study of flow field and drag coefficient of model and small natural trees in a wind tunnel. *Urban forestry & urban greening* 35, 230–239.
- Massman, W., 1987. A comparative study of some mathematical models of the mean wind structure and aerodynamic drag of plant canopies. *Boundary-layer meteorology* 40, 179–197.
- Mayhead, G., 1973. Some drag coefficients for British forest trees derived from wind tunnel studies. *Agricultural meteorology* 12, 123–130.
- Mochida, A., Tabata, Y., Iwata, T., Yoshino, H., 2008. Examining tree canopy models for CFD prediction of wind environment at pedestrian level. *Journal of Wind Engineering and Industrial Aerodynamics* 96, 1667–1677.
- Molina-Aiz, F., Valera, D., Álvarez, A., Madueño, A., 2006. A wind tunnel study of airflow through horticultural crops: determination of the drag coefficient. *Biosystems engineering* 93, 447–457.
- Moradpour, M., Afshin, H., Farhanieh, B., 2017. A numerical investigation of reactive air pollutant dispersion in urban street canyons with tree planting. *Atmospheric Pollution Research* 8, 253–266.
- Nebenführ, B., Davidson, L., 2015. Large-eddy simulation study of thermally stratified canopy flow. *Boundary-layer meteorology* 156, 253–276.
- Oke, T.R., 1989. The micrometeorology of the urban forest. *Philosophical Transactions of the Royal Society of London. B, Biological Sciences* 324, 335–349.
- Oke, T.R., Mills, G., Christen, A., Voogt, J.A., 2017. *Urban climates*. Cambridge university press.
- Owens, S.O., Majumdar, D., Wilson, C.E., Bartholomew, P., van Reeuwijk, M., 2024. A conservative immersed boundary method for the multi-physics urban large-eddy simulation model uDales v2.0. *EGUsphere* 2024, 1–33.
- Raupach, M.R., Finnigan, J.J., Brunet, Y., 1996. Coherent eddies and turbulence in vegetation canopies: the mixing-layer analogy. *Boundary-Layer Meteorology 25th Anniversary Volume, 1970–1995: Invited Reviews and Selected Contributions to Recognise Ted Munn's Contribution as Editor over the Past 25 Years*, 351–382.
- Ricci, A., Guasco, M., Caboni, F., Orlanno, M., Giachetta, A., Repetto, M., 2022. Impact of surrounding environments and vegetation on wind comfort assessment of a new tower with vertical green park. *Building and Environment* 207, 108409.
- Rudnicki, M., Mitchell, S.J., Novak, M.D., 2004. Wind tunnel measurements of crown streamlining and drag relationships for three conifer species. *Canadian Journal of Forest Research* 34, 666–676.
- Salim, M.H., Schlünzen, K.H., Grawe, D., 2015. Including trees in the numerical simulations of the wind flow in urban areas: Should we care? *Journal of Wind Engineering and Industrial Aerodynamics* 144, 84–95.
- Santiago, J.L., Martilli, A., Martin, F., 2017. On dry deposition modelling of atmospheric pollutants on vegetation at the microscale: Application to the impact of street vegetation on air quality. *Boundary-layer meteorology* 162, 451–474.
- Sanz, C., 2003. A note on $k-\epsilon$ modelling of vegetation canopy air-flows. *Boundary-Layer Meteorology* 108, 191–197.
- Shaw, R., Den Hartog, G., King, K., Thurtell, G., 1974. Measurements of mean wind flow and three-dimensional turbulence intensity within a mature corn canopy. *Agricultural Meteorology* 13, 419–425.
- Shaw, R.H., Schumann, U., 1992. Large-eddy simulation of turbulent flow above and within a forest. *Boundary-Layer Meteorology* 61, 47–64.
- Shu, C., Wang, L.L., Mortezaadeh, M., 2020. Dimensional analysis of Reynolds independence and regional critical Reynolds numbers for urban aerodynamics. *Journal of Wind Engineering and Industrial Aerodynamics* 203, 104232.
- Smith, M.M., Bentrup, G., Kellerman, T., MacFarland, K., Straight, R., Ameyaw, L., 2021. Windbreaks in the United States: A systematic review of producer-reported benefits, challenges, management activities and drivers of adoption. *Agricultural Systems* 187, 103032.
- Suter, I., Grylls, T., Sützl, B.S., Owens, S.O., Wilson, C.E., van Reeuwijk, M., 2022. uDales 1.0: a large-eddy simulation model for urban environments. *Geoscientific Model Development* 15, 5309–5335.
- Svensson, U., Häggkvist, K., 1990. A two-equation turbulence model for canopy flows. *Journal of wind engineering and industrial aerodynamics* 35, 201–211.
- Vollsinger, S., Mitchell, S.J., Byrne, K.E., Novak, M.D., Rudnicki, M., 2005. Wind tunnel measurements of crown streamlining and drag relationships for several hardwood species. *Canadian Journal of Forest Research* 35, 1238–

1249.

- Vranckx, S., Vos, P., Maiheu, B., Janssen, S., 2015. Impact of trees on pollutant dispersion in street canyons: A numerical study of the annual average effects in antwerp, belgium. *Science of the Total Environment* 532, 474–483.
- Vreman, A., 2004. An eddy-viscosity subgrid-scale model for turbulent shear flow: Algebraic theory and applications. *Physics of fluids* 16, 3670–3681.
- Wang, Z.Y., Plate, E.J., Rau, M., Keiser, R., 1996. Scale effects in wind tunnel modelling. *Journal of Wind Engineering and Industrial Aerodynamics* 61, 113–130.
- Weninger, T., Scheper, S., Lackóová, L., Kitzler, B., Gartner, K., King, N., Cornelis, W., Strauss, P., Michel, K., 2021. Ecosystem services of tree windbreaks in rural landscapes—a systematic review. *Environmental Research Letters* 16, 103002.
- Wilson, J., Ward, D., Thurtell, G., Kidd, G., 1982. Statistics of atmospheric turbulence within and above a corn canopy. *Boundary-Layer Meteorology* 24, 495–519.
- Wilson, J.D., 1985. Numerical studies of flow through a windbreak. *Journal of Wind Engineering and Industrial Aerodynamics* 21, 119–154.
- Yang, A.S., Juan, Y.H., Wen, C.Y., Chang, C.J., 2017. Numerical simulation of cooling effect of vegetation enhancement in a subtropical urban park. *Applied energy* 192, 178–200.

Table A.2: Typical values of drag coefficient and leaf-area density reported/used in literature for different vegetation canopies.

Reference	Type	C_d^V [-]	a [m^{-1}]	ℓ_d [m]
Field experiments of tree canopies				
Baldocchi and Meyers (1988)	deciduous	0.15 ^b	0.28 ^a	23.61
Amiro (1990)	aspen	0.14 ^a	0.43 ^a	16.67
	pine	0.171 ^a	0.166 ^a	35.06
	spruce	0.13 ^a	1.59 ^a	4.85
	spruce	0.2 ^b	0.57 ^a	8.77
Gardiner (1994)	spruce	0.2 ^b	0.57 ^a	8.77
Katul et al. (2004)	spruce	0.2	1.0	5.0
	aspen	0.2	0.4	12.5
	jack pine	0.2	0.133	37.5
	scots pine	0.2	0.13	38.5
	loblolly pine	0.2	0.237	21.05
	hardwood forest	0.15	0.227	29.33
Field/wind-tunnel experiments of low vegetation				
Shaw et al. (1974); Massman (1987)	corn canopy	0.17	1.14 ^a	5.15
Wilson et al. (1982)	corn canopy	0.17	3.03 ^a	1.94
Katul et al. (2004)	rice canopy	0.3	4.31	0.77
	corn canopy	0.3	1.32	2.53
Molina-Aiz et al. (2006) ^c	tomato	0.26	5.6, 8.2, 11.7	0.69, 0.47, 0.33
	sweet pepper	0.23	5.8, 10.6, 12.6	0.75, 0.41, 0.34
	aubergine	0.23	3.7, 6.7, 11.6	1.17, 0.65, 0.37
	bean	0.22	3.6, 5.8, 6.8	1.26, 0.78, 0.67
Numerical simulations of vegetation canopies				
Li et al. (1985)	pine forest, corn canopy	0.165	0.71 ^a , 1.06 ^a	8.54, 5.72
Shaw and Schumann (1992)	deciduous forest	0.15	1.99 ^a , 5.04 ^a	3.34, 1.32
Svensson and Häggkvist (1990)	corn canopy, orchard	0.3	0.5, 2.1	6.67, 1.59
Liang et al. (2006)	trees in an urban area	0.2	0.4 - 0.75	12.5 - 6.67
Belcher et al. (2008)	open woodland to dense spruce plantation	0.25	0.1 - 1.0	40.0 - 4.0
Amorim et al. (2013)	trees in an urban area	0.2	1.0	5.0
Kenjereš and ter Kuile (2013)	trees in an urban area	0.1	1.0, 3.0	10.0, 3.33
Gromke and Blocken (2015a,b)	trees in an urban area	0.2	1.0	5.0
Gromke et al. (2015)	trees in an urban area	0.2	0.55, 0.75, 1.5	9.1, 6.67, 3.33
Krayenhoff et al. (2015)	trees in an urban area	0.2	0.06 - 0.5	83.33 - 10
Vranckx et al. (2015)	trees in an urban area	0.15, 0.33	1.6, 4.0	4.17, 1.89, 0.76
Ghasemian et al. (2017)	trees in an urban area	0.6	0.17, 0.42, 1.0, 1.25, 3.33	9.8, 3.97, 1.67, 1.33, 0.5
Jeanjean et al. (2017)	trees in an urban area	0.25	0.0, 1.06, 1.6	∞ , 3.85, 2.5
Moradpour et al. (2017)	trees in an urban street canyon	0.2	0.5 - 2.0	10.0 - 2.5
Santiago et al. (2017)	trees in an urban area	0.2	0.0625, 0.125, 0.25	80.0, 40.0, 20.0
Yang et al. (2017)	trees in subtropical urban park	0.2	1.0, 4.0	5.0, 1.25
Grylls and van Reeuwijk (2021, 2022)	trees in an urban area	0.2	1.0	5.0
Ricci et al. (2022)	trees in an urban area	0.3	1.0 - 3.0	3.33 - 1.11
Duan et al. (2024)	trees in an urban area	0.1, 0.2	2.5, 1.0	4.0, 5.0
Fu et al. (2024)	trees in an urban area	0.2	2.2, 1.8, 1.6, 1.4,	2.27, 2.78, 3.12,
			1.0, 0.6, 0.2	3.57, 5.0, 8.33, 25.0

^a average value calculated based on the profile given in the article^b taken based on other literature of similar vegetation type^c this study was carried out in wind tunnel

Table A.3: Estimated drag length for wind-tunnel model trees from literature.

Reference	Description	C_d [-]	α_L [-]	U_∞ [m/s]	L [m]	W [m]	H [m]	$\hat{\ell}_d$ [m]
Grant and Nickling (1998)	artificial Scots pine Christmas tree							
	- least porous	1.2 ^a	0.51 ^b	–	0.3 ^c	0.3	1.45	0.173
	- medium porous	1.07 ^a	0.63 ^b	–	0.3 ^c	0.3	1.45	0.299
	- most porous	0.865 ^a	0.69 ^b	–	0.3 ^c	0.3	1.45	0.402
Guan et al. (2003)	model no. 1	1.06 ^a	0.133	1.6 – 5.3	0.14	0.5	0.1	0.015
	model no. 2	0.94 ^a	0.303	1.6 – 5.3	0.14	0.5	0.1	0.038
	model no. 3	0.84 ^a	0.401	1.6 – 5.3	0.1	0.5	0.1	0.034
	model no. 4	0.81 ^a	0.450	1.6 – 5.3	0.1	0.5	0.1	0.043
	model no. 5	0.74 ^a	0.503	1.6 – 5.3	0.1	0.5	0.1	0.054
	model no. 6	0.67 ^a	0.605	1.6 – 5.3	0.1	0.5	0.1	0.086
	model no. 7	0.6 ^a	0.685	1.6 – 5.3	0.1	0.5	0.1	0.128
Bitog et al. (2011) ^e	<i>Pinus thunbergii</i>							
	– one tree	0.55	0.91	2.0 – 8.0	1.0	1.0	1.7	7.34
	– two tree	0.82	0.69	2.0 – 8.0	1.0	1.0	1.7	1.53
	– three tree	1.08	0.42	2.0 – 8.0	1.0	1.0	1.7	0.5
Lee et al. (2014)	<i>Abies concolor</i>							
	– control	–	0.2985	5.0	0.11 ^c	0.11	0.19	0.033
	– rotated	–	0.344	5.0	0.11 ^c	0.11	0.19	0.04
	– no leaf	–	0.8782	5.0	0.11 ^c	0.11	0.19	0.568
Manickathan et al. (2018)	model tree 1	0.58	0.102 ^b	3.0–20.0	0.04 ^c	0.04 ^d	0.12	0.003
	model tree 2	0.68	0.219 ^b	3.0–20.0	0.082 ^c	0.082 ^d	0.10	0.019
	model tree 3	0.70–0.75	0.448 ^b	3.0–20.0	0.114 ^c	0.114 ^d	0.21	0.062
	<i>Chamaecyparis</i>	0.72–0.87	0.381 ^b	3.0–20.0	0.119 ^c	0.119 ^d	0.25	0.048
	<i>pisifera</i>							
	<i>Ilex crenata</i>	0.87	0.382 ^b	3.0–20.0	0.128 ^c	0.128 ^d	0.32	0.05
	<i>Ilex crenata</i> – de- foliated	0.31–0.33	0.871 ^b	3.0–20.0	0.128 ^c	0.128 ^d	0.32	0.606
Fellini et al. (2022)	single model tree	1.07	0.3	4.0–24.0	0.045	0.045	0.065	0.014

^a C_d was calculated based on the streamwise velocity at canopy crown height $\langle \bar{u} \rangle_{y|z=H}$, instead of U_∞ ^b α_L was calculated from optical porosity (α_O) at quiescent condition as $\alpha_L = \alpha_O^{0.4}$ (Guan et al., 2003)^c L was not mentioned in the particular literature, hence takes same as W ^d W was not mentioned in the particular literature, hence calculated in a way that $W \times H$ matches the mentioned projected frontal area.^e this study considered full-scale tree models